



ELSEVIER

Contents lists available at ScienceDirect

Applied Thermal Engineering

journal homepage: www.elsevier.com/locate/apthermeng

Research Paper

Geometry and nanoparticle loading effects on the bio-based nano-PCM filled cylindrical thermal energy storage system

Soroush Ebadi, Syeda Humaira Tasnim, Amir Abbas Aliabadi, Shohel Mahmud*

School of Engineering, University of Guelph, Guelph, ON, Canada

HIGHLIGHTS

- Melting process of bio-based nano-PCM is investigated inside cylindrical geometry.
- CuO nanoparticles are dispersed in coconut oil PCM to prepare the nano-PCM.
- Thermal conductivity of nano-PCM is improved by 7.5% for wt.% = 1.
- Melt fraction (MF) of nano-PCM is improved by 15% for wt.% = 0.0218.
- MF is calculated using interface tracking from digital images with maximum uncertainty of $\pm 6.7\%$.

ARTICLE INFO

Keywords:

Thermal energy storage system
Nanoparticles
Phase change material
Melt fraction
Thermal conductivity enhancement

ABSTRACT

Dispersing highly conductive nanoparticles into a Phase Change Material (PCM) is one of the effective methods to increase thermal conductivity and decrease the required time for phase change in thermal energy storage systems. The current work reports an experimental effort to investigate the detailed melting process of a nano-PCM inside a Cylindrical Thermal Energy Storage (C-TES) system. The experimental setup consists of two vertical C-TES systems and a constant temperature bath. One of the C-TES systems is filled with a bio-based pure PCM (coconut oil) and the second one is filled with a nano-PCM (CuO nanoparticles dispersed in coconut oil PCM). The objective of this study is to investigate the effects of (i) height of the PCM, (ii) temperature of the hot wall, and (iii) weight fractions of nanoparticles on the melting of nano-PCM. The thermophysical properties of nano-PCM are measured and reported in this paper. Digital images of melting front and temperatures at selected locations are captured at three pre-selected boundary temperatures and four weight fractions of nanoparticles and presented. Image processing of photographs along with numerical integration is used to calculate melt fraction. To facilitate a better comparison of melting pattern between bio-based PCM and nano-PCM, solid–liquid interface is presented on the XY plots. Results show that at the beginning of the melting process, pure PCM and nano-PCM behave almost the same, however, with an ongoing heating process, nano-PCMs melt faster than pure PCM. The height of the PCM and hot wall temperature affect the melting pattern and melting time, respectively. An extensive analysis is reported as well to show how to calculate the uncertainty associated with image based melt fraction calculation.

1. Introduction

Nowadays, one of the main environmental concerns is the increase in the amount of greenhouse gas emissions due to the widespread use of fossil fuels. Such greenhouse emissions have a significant impact on the global warming. The global warming concern leads to efforts for developing systems that utilize energy sources more effectively. One of the major solutions to this concern is storing energy efficiently, which can be transformed to the required form necessary for subsequent operations. Storing energy can play a significant role to balance the

amount of demand and supply, reduce the level of carbon dioxide (CO₂) emissions from burning fossil fuels, and play a vital role in conserving energy [1]. Thermal Energy Storage (TES) systems have been developed for storing thermal energy by heating or cooling a specific medium. TES systems have been used in many different applications including heating and cooling purposes or generating power. TES systems are divided into three major groups: (i) Sensible Heat Thermal Energy Storage (SHTES), (ii) Latent Heat Thermal Energy Storage (LHTES) and (iii) Thermo-Chemical Energy Storage (TCES) systems. The SHTES system is based on raising (or lowering) the temperature by heating (or

* Corresponding author.

E-mail address: smahmud@uoguelph.ca (S. Mahmud).<https://doi.org/10.1016/j.applthermaleng.2018.05.091>

Received 22 September 2017; Received in revised form 25 April 2018; Accepted 24 May 2018

Available online 08 June 2018

1359-4311/ © 2018 Elsevier Ltd. All rights reserved.

Nomenclature

c_p	specific heat at constant pressure [kJ/kg K]
D	inner diameter of C-TES system [cm]
g	gravitational acceleration [m/s ²]
h	latent heat of fusion [kJ/kg]
H_0	height of the C-TES system [cm]
H	height of the filled PCM in C-TES system [cm]
K	thermal conductivity [W/m K]
N_{px}	number of pixel in a particular direction
T	temperature [°C]
T_{C1}	final temperature measurement at thermocouple location #1 [°C]
T_{C2}	final temperature measurement at thermocouple location #2 [°C]
T_{DQ}	temperature measured by DAQ system [°C]
T_h	hot wall temperature [°C]
T_m	melting temperature of PCM [°C]
T_{TC}	temperature measured by thermocouple [°C]
T_{RG}	temperature measured by thermal regulator [°C]
V	volume of the PCM/nano-PCM [m ³]
wt.%	percentage of nanoparticles volume fraction

Greek symbols

α	coefficient of thermal diffusivity [m ² /s]
β	coefficient of thermal expansion [1/K]
δT_{TC}	accuracy of thermocouple [°C]

δT_{DQ}	accuracy of DAQ system [°C]
δT_{RG}	accuracy of thermal regulator [°C]
δH	accuracy of height gage [mm]
δD	accuracy of digital caliper [mm]
δx	accuracy of the interface location in the x-direction [pixel]
δy	accuracy of the interface location in the y-direction [pixel]
$\delta \bar{x}$	accuracy of the area center in the x-direction [pixel]
μ	dynamic viscosity [Pa s]
ρ	density [kg/m ³]

Subscripts

h	hot
m	melt

Abbreviation

C-TES	cylindrical thermal energy storage
DAQ	data acquisition
LHTES	latent heat thermal energy storage system
MF	melt fraction
PCM	phase change material
Ra	Rayleigh number
RSS	Root sum squared
RT	Rubitherm
SHTES	sensible heat thermal energy storage system
TCES	thermo-chemical thermal energy storage system
TES	thermal energy storage

cooling) of a liquid or solid storage medium, while LHTES uses Phase Change Materials (PCMs) to store (or release) thermal energy during the PCM's melting (or solidification) process. In other words, thermal energy will be absorbed (i.e., the charging process) by a PCM during its melting stage if a thermal source with the temperature higher than the melting point of PCM is exposed to the LHTES system. Similarly, thermal energy will be released (i.e., the discharging process) by a PCM during its solidification stage if a thermal sink with a temperature lower than the melting point of PCM is exposed to the LHTES system. The LHTES system has two main advantages over SHTES systems: (i) higher energy storage density and (ii) smoother temperature fluctuations [2]. It is already shown that a LHTES system has the potential of storing thermal energy 5–14 times higher than SHTES systems [1]. The TCES system benefits from a specific chemical reaction in order to release or store heat and the amount of heat stored relies on the quantity of storage medium, endothermic heat of reaction, and the bound of conversion [1]. The most common PCMs are paraffin waxes, hydrated salts, and organic/non-organic compounds, which have been used in a wide variety of applications based on their melting temperatures and heat capacities. For instance, PCM with melting temperature below 15 °C can be used in air conditioning systems for generating cooling, while a PCM with the melting temperature in a range 15–90 °C can be used for heating applications. However, traditional PCMs have several practical limitations including low thermal conductivity, which leads to low heat transfer rate during charging and discharging, weak thermal stability, and immature sub-cooling effect [3]. In order to enhance the thermal conductivity of a PCM, various methods can be used including dispersing highly conductive nanoparticles in PCM (nano-PCM), inserting metal fins, using porous materials, and use of foams [4]. Due to adding nanoparticles at different weight/volume fractions to a PCM, sedimentation can occur with time (more likely at high weight/volume fractions). As a result of sedimentation, the ability of enhancing thermal conductivity will be degraded as time furthers [5,6] which may pose a challenge to nano-PCM TES systems. To decrease the amount of sedimentation, different methods, such as, application of intensive

ultrasonic vibration to nano-PCM using an ultrasonic vibrator [6] and use of different surfactants [6,7] have been utilized.

Convection and conduction are the major modes of heat transfer encountered during charging and discharging processes, which are greatly influenced by the geometric and compositional properties of a LHTES system. Different types of geometries including rectangular, cylindrical, and spherical have been used for a TES system. For required specific applications, cylindrical enclosures can be used both vertically and horizontally [8]. This is the reason why cylindrical enclosure geometry is chosen for the present study. By surveying the literature, it can be found that a considerable number of published works are available regarding the use of cylindrical enclosures for a TES system.

Starting with horizontal cylindrical TES systems, Jourabian et al. [9] applied Lattice Boltzmann method to observe the effect of adding copper nanoparticles to water during a melting process. It is reported that increasing the amount of nanoparticles enhanced the melting rate but decreased the latent heat of fusion. The effect of adding copper oxide nanoparticles to n-octadecane PCM is studied both numerically and experimentally by Dhaidan et al. [10]. Authors reported an improvement in charging process at a lower amount of nanoparticles due to the effect of increasing viscosity and sedimentation. The volumetric heat generation effect during the phase change process of Rubitherm-27 (RT-27) and copper nanoparticles was performed by Bechiri and Mansouri [11]. The heat generation effect is identified less significant for high volume fractions of nanoparticles.

Regarding the use of vertical cylindrical enclosures, various research works are reported in the literature, mainly with pure PCM. For example, Jourabian and Farhadi [12] studied the convection melting of ice with copper nanoparticles in a vertical semi-circular enclosure and concluded that adding nanoparticles increased the thermal conductivity and reduced the latent heat of fusion. Zheng et al. [13] observed reduction in the natural convection due to adding carbon nanotubes inside a PCM filled vertical cylindrical enclosure heated from the bottom. Sciacovelli et al. [14] studied the effect of adding copper nanoparticles on the melting process inside a vertical single shell and tube heat

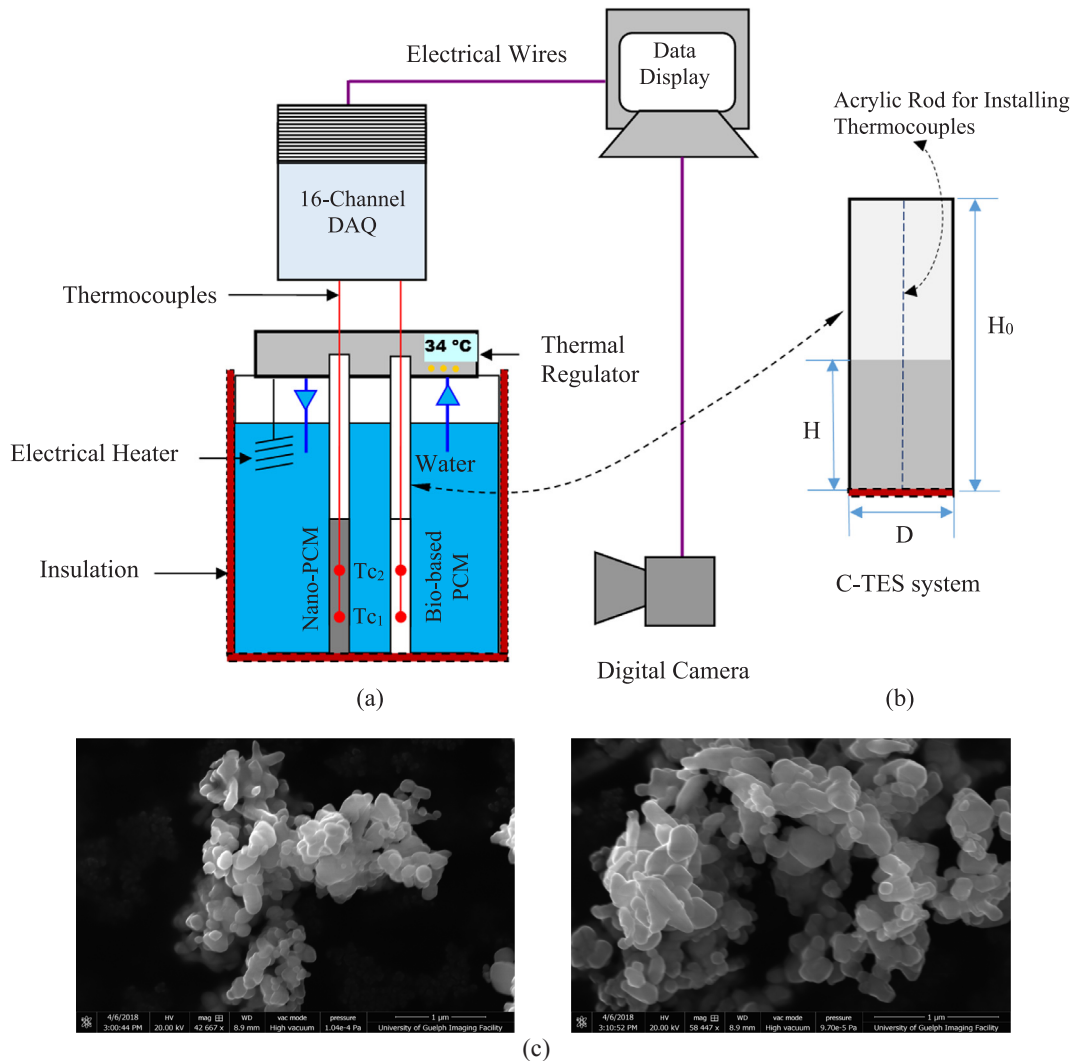


Fig. 1. Schematic diagram of (a) experimental setup (b) C-TES system, and (c) SEM images of CuO nanoparticles.

Table 1
Thermophysical properties of nanoparticles, PCM, and nano-PCM.

Properties (units)	CuO nanoparticles [10]	Coconut Oil (Measured)			
		Solid (15 °C)	Liquid (32 °C) (wt. % = 0.0)	Liquid (32 °C) (wt. % = 0.1)	Liquid (32 °C) (wt. % = 1.0)
ρ (kg/m ³)	6510.0	920	914	916	922
μ (Pa s)	–	–	0.0326	0.0332	0.362
c_p (J/kg K)	540	3750	2010	2001	1995
k (W/m K)	18.0	0.228	0.166	0.174	0.290
h_f (kJ/kg)	–	–	103	101	94.5
T_m (ΔT_m)	–	24 °C (\pm 1 °C)			

exchanger. It was concluded that by using nano-PCM with the volume fraction of 4% the melting time is reduced up to 15%. A numerical study on the melting process of RT-27 in a vertical circular tube was performed by Shamueli et al. [15] and later verified with previous experiments. The authors investigated the effect of a mushy zone parameter on the melting process. It was observed that experimental melting patterns were predicted closely by the numerical simulation when the mushy zone parameter was set equal to 10⁸. An experimental investigation of the melting process of n-eicosane using a vertical cylindrical enclosure was performed by Sparrow and Broadbent [16]. It

was reported that sub-cooling had a significant delaying impact on the melting process and reduced the rate of energy transfer required for melting. An analytical study of contact melting of a PCM in a vertical cylindrical capsule was conducted by Wenzhen et al. [17]. In this research, capsules were filled by eicosanoid as a PCM and heated isothermally from the bottom and sides. To investigate the rate of heat transfer through the contact liquid layer, the liquid film theory was used. The authors found that reducing aspect ratio was beneficial to increase the melting rate. Jones et al. [18] performed experimental and numerical studies of melting of n-eicosane as a PCM in a vertical cylindrical container. The authors reported that four melting regimes could occur during the melting process including (i) pure conduction, (ii) mixed convection and conduction, (iii) convection dominant, and (iv) shrinking solid. In an extensive numerical analysis, Ebadi et al. [19] concluded that nano-PCM with higher volume fractions of nanoparticles improve the melt fraction and convection heat transfer coefficient but reduce both sensible and latent heat capacities of nano-PCM inside a cylindrical thermal energy storage system.

Current literature indicates that a noticeable number of technical articles deal with the phase change processes of PCM inside enclosures with various shapes (e.g., [8]), while the study with regard to nano-PCM in enclosed space is limited (e.g., [4]), specifically, inside an open top vertical cylindrical enclosures with adiabatic bottom and isothermal side wall boundary conditions. This limitation in the current literature is the primary motivation behind the present study. Authors



Fig. 2. Visualization comparison of bio-based PCM (wt.% = 0) and different nanoparticles weight fractions (wt.% = 0.0156, 0.0218, and 0.0311), H = 7.2 cm.

used a bio-based edible coconut oil PCM ($T_m = 24\text{ }^\circ\text{C}$) instead of paraffin- and petro-based PCMs (e.g., n-octadecane, n-eicosane), widely used in TES researches and reported extensively in the literature (e.g., [20,21]). Paraffin- and petro-based PCMs exhibit excellent time transition characteristics (can be observed from their T-history curve) and ideal for many TES researches, but stability and sedimentation are widely reported limitations for such PCMs. In contrast, edible coconut oil PCM exhibits greater stability and less sedimentation with CuO nanoparticles, although the time transition characteristic feature for this PCM is not as ideal as paraffin- and petro-based PCMs. Furthermore, the coconut oil is less expensive, widely available, and having a

melting temperature close to the typical room/lab temperature. A comprehensive experimental study is performed to study the melting process of bio-based nano-PCM inside vertical cylindrical enclosure which is a representative geometry of a thermal energy storage system. Effect of nanoparticle loading, boundary wall temperature, and height of the PCM/nano-PCM inside C-TES system on the melting process and temperature distribution is reported. An extensive analysis is reported as well to show how to calculate the uncertainty associated with image based melt fraction calculation.

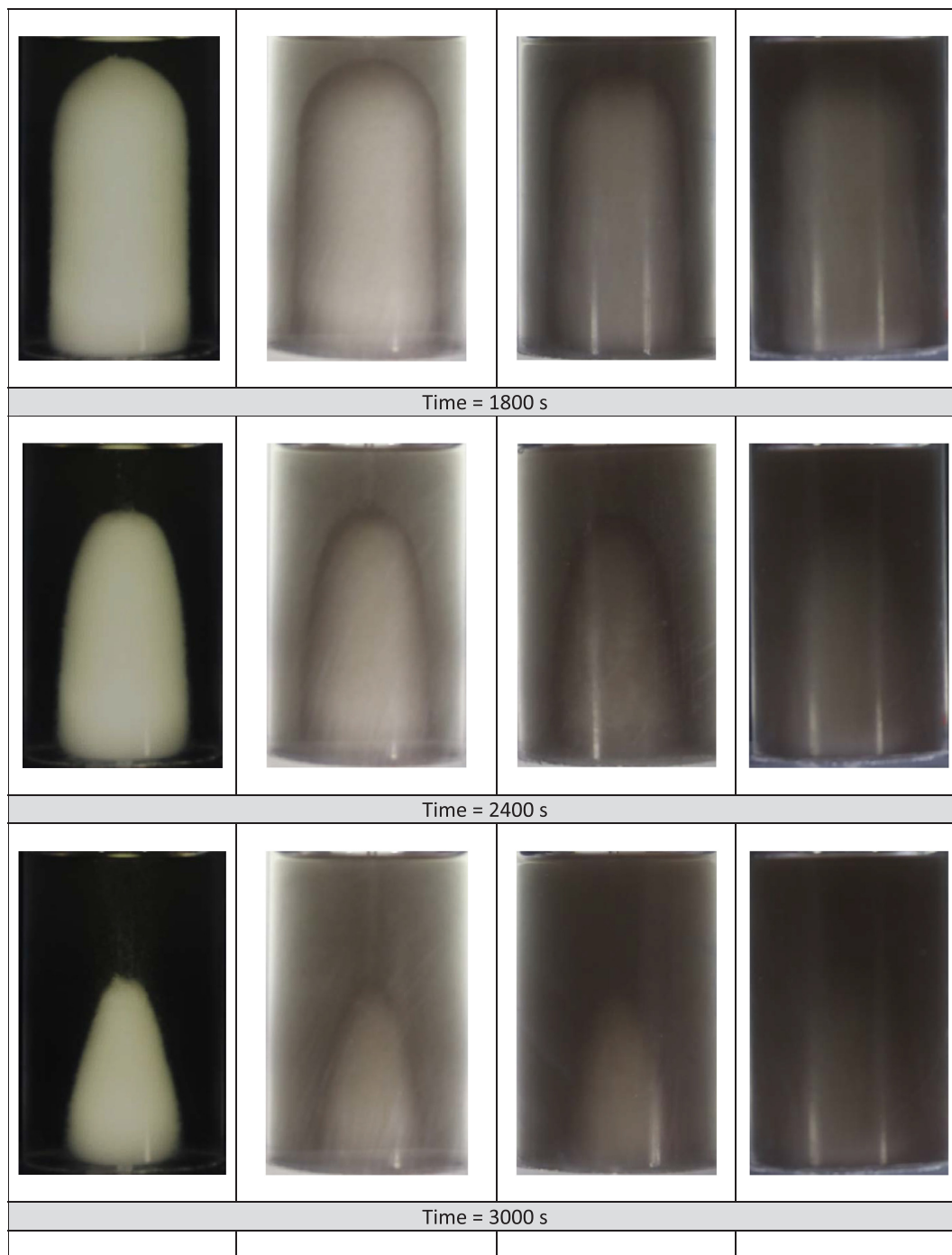


Fig. 2. (continued)

2. Experimental work

In this section, a detailed description of the prototype cylindrical thermal energy storage (C-TES) system, preparation of nano-PCM, and experimental procedure are presented.

2.1. C-TES prototype system

To visualize the melting process of pure PCM and nano-PCM and to measure the temperature distribution at selected locations, an experimental setup and multiple prototype C-TES systems were constructed. Each C-TES prototype consisted of two transparent acrylic pipes with the height (H_0) of 33 cm, inner diameter (D) of 4.44 cm, and thickness

of 0.3 cm (see Fig. 1(a) and (b)). Both pipes were attached to a 2.5 cm thick acrylic plate vertically with transparent acrylic cement (manufacturer: Scigrip). The center-to-center distance between the pipes is 14 cm. In the center of each pipe, a thin transparent acrylic rod of 3.23 mm diameter was installed vertically, where T-type thermocouples (manufacturer: Omega) at different heights (i.e., 15 mm and 35 mm from the bottom) were installed firmly. These pipes were kept open from the top to avoid having any pressure build up on the bio-based PCM and nano-PCM during melting experiments. The bottom part of the C-TES prototype was properly insulated. During each experiment, one of the C-TES system was filled with a bio-based PCM (coconut oil) and the second one was filled with a nano-PCM (copper oxide nanoparticles dispersed in coconut oil PCM).

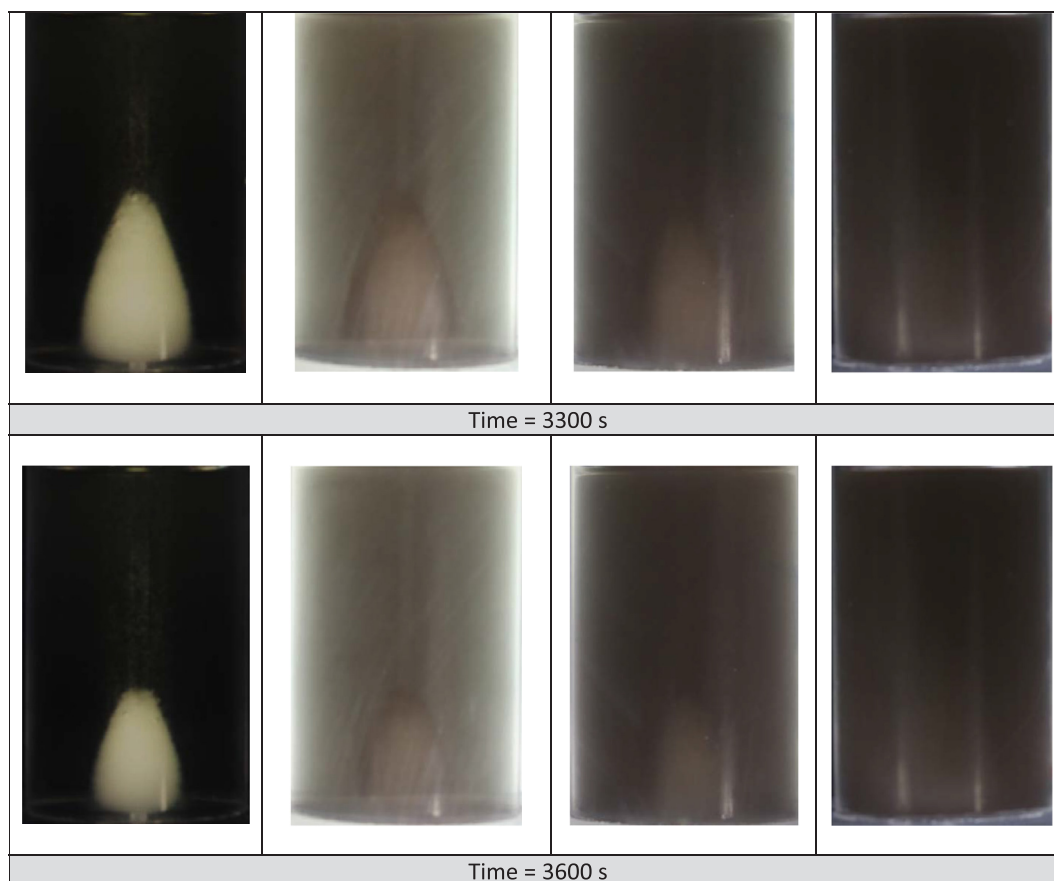


Fig. 2. (continued)

2.2. Description of experimental setup

The main parts of the experimental setup consist of : (i) a $30\text{ cm} \times 30\text{ cm} \times 30\text{ cm}$ acrylic water tank (with the thickness of 8 mm), which is filled with deionized water, (ii) an immersion water heater with precision temperature controller (model: HCTB-3020, manufacturer : Omega) to create an isothermal environment, (iii) a recirculation pump to circulate water for maintaining uniform temperature, (iv) T-type thermocouples, (v) a 16-channel DAQ system (model : NI9213, manufacturer: National Instruments), and (vi) a digital camera (model: EOS rebel T5, manufacturer: Canon) to capture images periodically. The immersion heater was installed at one end of the water tank while the prototype C-TES system was placed on the other end. A barrier, made of an acrylic sheet ($30\text{ cm} \times 20\text{ cm}$), was placed between the immersion heater and the C-TES prototype to avoid convection and turbulent effects associated with direct water movement. A 5 cm gap was maintained between the barrier and the bottom surface of the water tank to allow hot water circulated around the C-TES system to have a uniform temperature for the experiment. The temperature inside the water tank was regularly monitored at different locations to ensure that the appropriate isothermal boundary condition was achieved before collecting the data. In addition, to have clear images during the melting process, a part of the barrier was painted white (for nano-PCM) and another part was black (for pure PCM). A schematic of the experimental setup is shown in Fig. 1(a), while the schematic of the C-TES system is shown in Fig. 1(b).

2.3. Nano-PCM preparation

For the current experimental work, the Copper (II) Oxide (CuO) nanoparticles were purchased from Sigma-Aldrich in nanopowder form. Based on the information obtained from TEM analysis (provided by the

manufacturer), the particle size is $< 50\text{ nm}$. Thermophysical properties of the CuO nanoparticles are provided in Table 1. Images obtained from SEM analysis (Physics Department, University of Guelph) are given in Fig. 1(c), which provide further information on the nanoparticles shape.

The refined form of the bio-based coconut oil was obtained from a local vegetable oil supplier. Thermophysical properties of pure coconut oil and nanoparticle enhanced coconut oil were measured in different labs at the University of Guelph. Following equipment/methods were used for property calculation:

- KD2 Pro and TPS-500 system (for thermal conductivity),
- Rotational Viscometer and Vibration Viscometer (for dynamic viscosity),
- DMA 35 Density meter (for liquid density),
- Differential Scanning Calorimeter (DSC) (for specific heat and heat of fusion), and
- Melting Point Apparatus MPS10 (for melting temperature).

Thermo-physical properties of CuO nanoparticles, pure PCM, and nano-PCM and are presented in Table 1.

Nano-PCM with different weight fractions of nanoparticles were prepared before experiments. Initially, a selected amount of coconut oil was melted and filled in a graduated beaker. At the next step, the required amount of nanoparticles to achieve a desired weight fraction was weighed by a precise balance (model: XP6, manufacturer: Mettler Toledo) and added to the PCM filled beaker. The mixture temperature was raised to $60\text{ }^\circ\text{C}$ and then stirred by a magnetic stirrer (model: SP88854100, manufacturer: Thermo Scientific) for 12 h. Subsequently, to improve the quality of the mixture and release the trapped air inside it, the mixing process was enhanced by using a sonicator (model: Q500, manufacturer: Qsonica) for 30 min. The prepared mixture of the nano-PCM was solidified by lowering its temperature below the melting

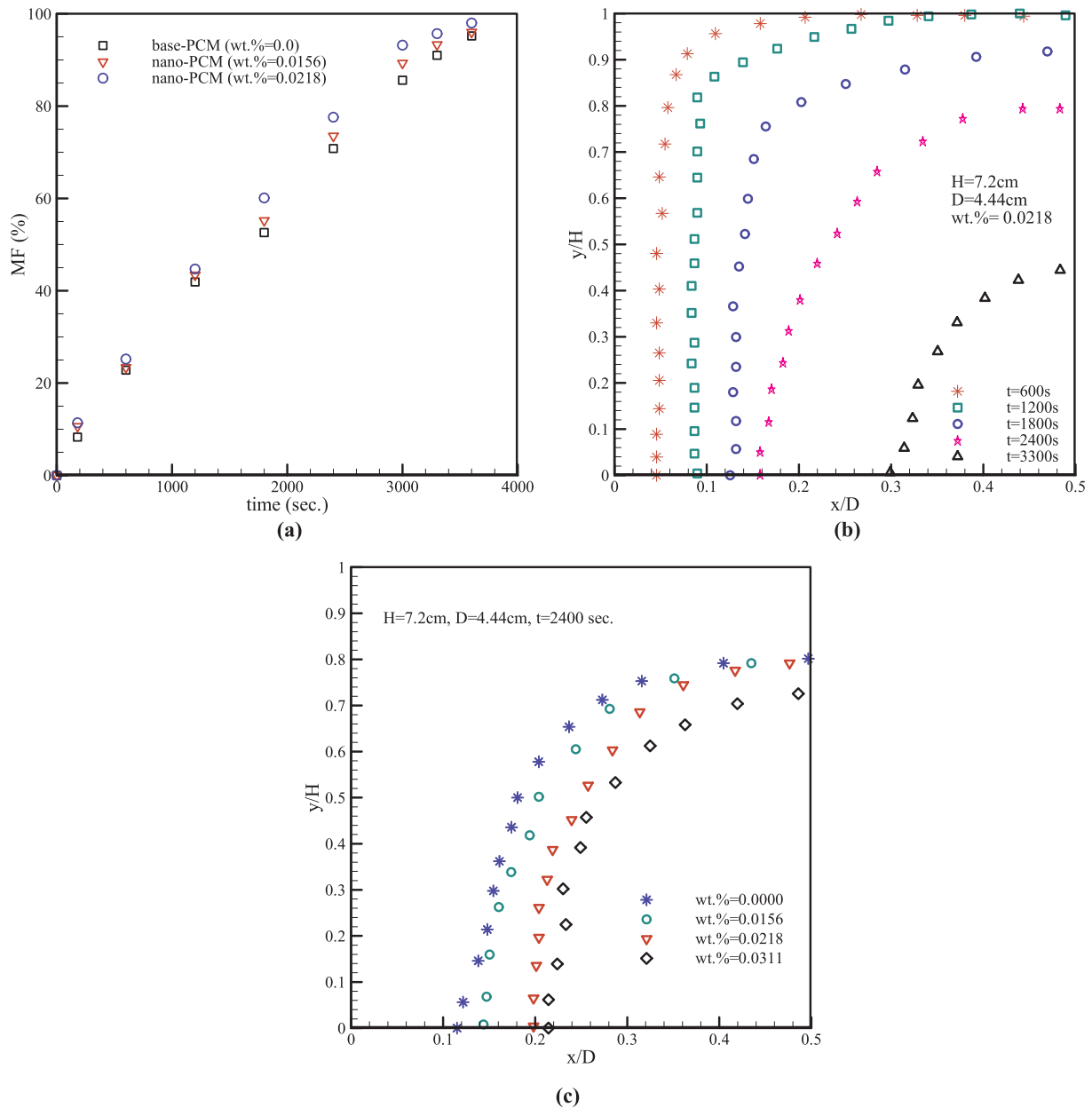


Fig. 3. (a) Transient variation of melt fraction for base-based PCM (wt.% = 0) and nano-PCM (wt.% = 0.0156 and 0.0218) when H = 7.2 cm and Th = 34 °C, (b) solid–liquid interface profiles as a function of time for wt.% = 0.0218 and H = 7.2 cm, and (c) solid–liquid interface profiles as a function of wt.% and t = 2400 s.

temperature in a second constant temperature bath. Subsequently, multiple cycles of melting and solidification process were executed and it was observed that the nano-PCM was stable and the amount of sedimentation was minimum. Then, the nano-PCM was poured into one of the enclosures at a specific height to represent a predetermined Rayleigh number.

2.4. Experimental procedure

The experimental work was carried out in several steps. At the beginning, for a given temperature difference (i.e., Th-Tm), the vertical height of the PCM (H) required to achieve a pre-selected Rayleigh number was calculated by using the following equations.

$$Ra = \frac{g(\rho\beta)H^3(T_h - T_m)}{\mu\alpha} \tag{1}$$

where ρ, β, μ, and α represent density, coefficient of thermal expansion,

dynamic viscosity, and coefficient of thermal diffusivity of bio-based PCM/nano-PCM, respectively. In addition, g is the gravitational acceleration, H is the height of filled bio-based PCM/nano-PCM, Th is the temperature of the hot bath, and Tm is the melting temperature.

Next, one of the prototype C-TES systems was filled with the liquid bio-based PCM and the second one with liquid nano-PCM at the calculated height. The bio-based PCM and nano-PCM filled prototype C-TES systems were solidified gradually and sub-cooled to 21 °C using a constant temperature bath. The temperature of the main water tank was set to Th (Th > Tm) using the temperature controller. The sub-cooled C-TES prototype was placed inside the water tank once the temperature reached to Th. To reduce the heat loss to the surrounding, the water tank was properly insulated. During the melting process, the temperature inside the bio-based PCM and nano-PCM were monitored at 10 s intervals and images were captured by the digital camera periodically to observe the melting pattern inside the C-TES systems.

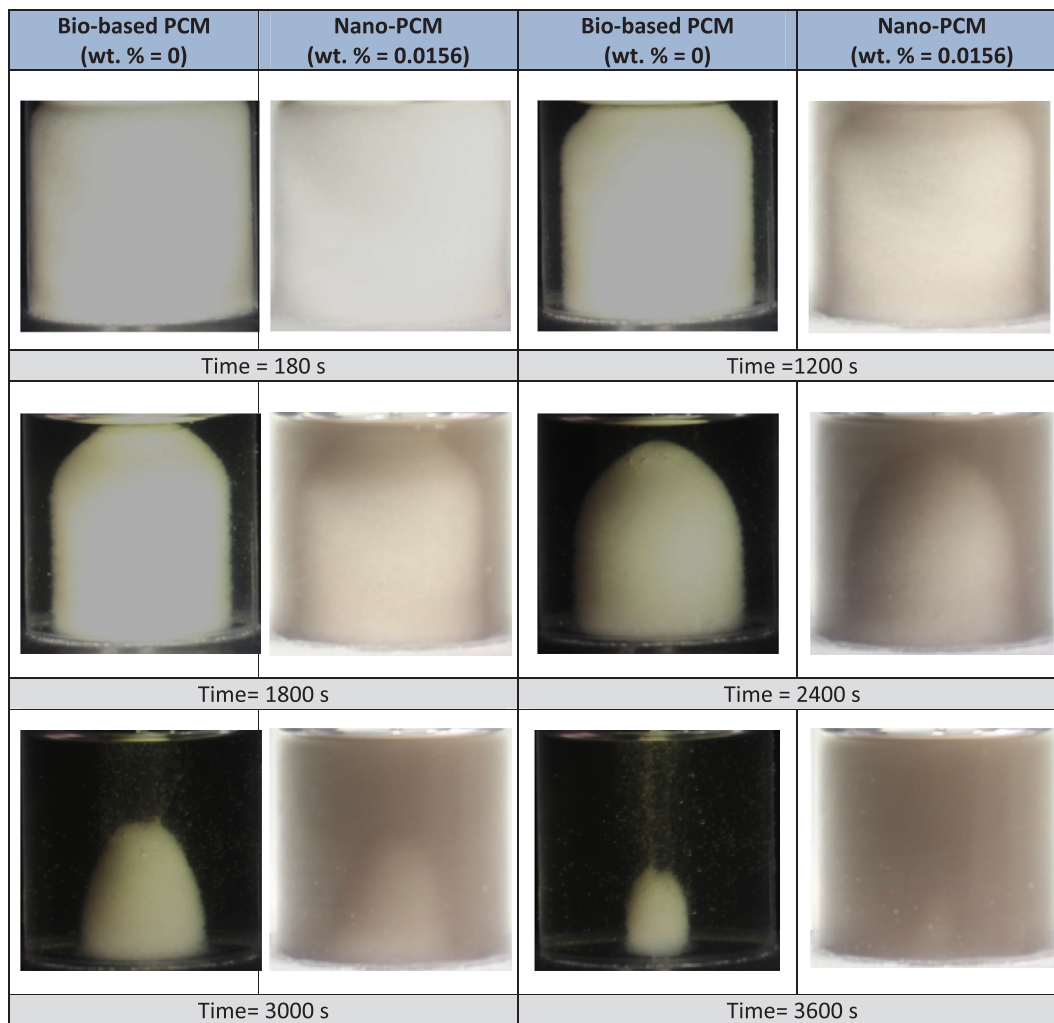


Fig. 4. Visualization comparison between bio-based PCM (wt.% = 0) and 0.0156 wt.% nano-PCM, H = 4 cm.

3. Results and discussion

In this section, selected results from the visualization experiments of pure PCM and nano-PCM are presented. For the nano-PCM, the selected weight fractions of nanoparticles ranges from 0 to 0.0311 wt.%, while the height of the PCM filled in C-TES systems is varied from 4 to 10 cm. Additionally, temperature distribution and melt fraction of the bio-based PCM and nano-PCM are presented.

3.1. Visualization Experiments: H = 7.2 cm and wt.% = 0.0156, 0.0218 and 0.0311

Fig. 2 shows the time evolution of the melting process of bio-based PCM and nano-PCM inside the C-TES system when the height of the bio-based PCM and nano-PCMs is 7.2 cm representing a Rayleigh number of 8.12×10^6 . Three different weight fractions of nanoparticles were considered, i.e., 0.0156 wt.%, 0.0218 wt.%, and 0.0311 wt.%, respectively. It is worth mentioning that low weight fractions are selected to ensure clear visualization of the melting pattern inside the C-TES system using nano-PCM as dispersion of CuO nanoparticles into the coconut oil makes it darker which poses difficulties during visualization, specifically, at higher weight fractions. By conducting several initial experiments using different weight fractions of CuO nanoparticles, it was identified that, tracking the melting pattern inside the C-TES system was difficult when the weight fraction was equal to or more than 0.0311 wt.%. Before each experiment, each C-TES system was kept in a

water bath at constant temperature of 21 °C for a prolonged period. Subsequently, this C-TES system was placed quickly inside the second bath where temperature of the water inside the second bath was previously set and maintained at pre-selected wall temperatures (i.e., 34 °C for Fig. 2). The melting process was tracked from the beginning until the bio-based PCM or nano-PCM was fully melted. The solid–liquid interface appeared few minutes after placing the C-TES system inside the water bath (e.g., with the temperature of 34 °C). Fig. 2 shows the captured images at eight selected time intervals. At the beginning of the melting process (180 s), conduction heat transfer dominated. Thermal energy transferred uniformly to the solid PCM and nano-PCM. A vertical thin layer of liquid PCM and nano-PCM was observed. The liquid layer took a shape of a concentric cylinder around the solid nano-PCM. However, it was difficult to differentiate the amount of melting from the visual observation at this stage. As time advanced, the thickness of the liquid layer increased in size. Motion in the liquid bio-based PCM (and nano-PCM) was established due to the onset of natural convection at the upper part of the C-TES system where the liquid layer was relatively wider than the lower part. However, at the lower part of the liquid layer conduction was still dominating as can be observed from the images at 600 s. With the advancement of time, the heated liquid layer of bio-based PCM close to the walls of the C-TES system raised due to its lower density. Due to the ongoing heating, the warm liquid PCM (both bio-based PCM and nano-PCM) accumulated at the top of the C-TES systems and exhibited high temperature due to the thermal stratification effect. As a result, more deformation was observed along the

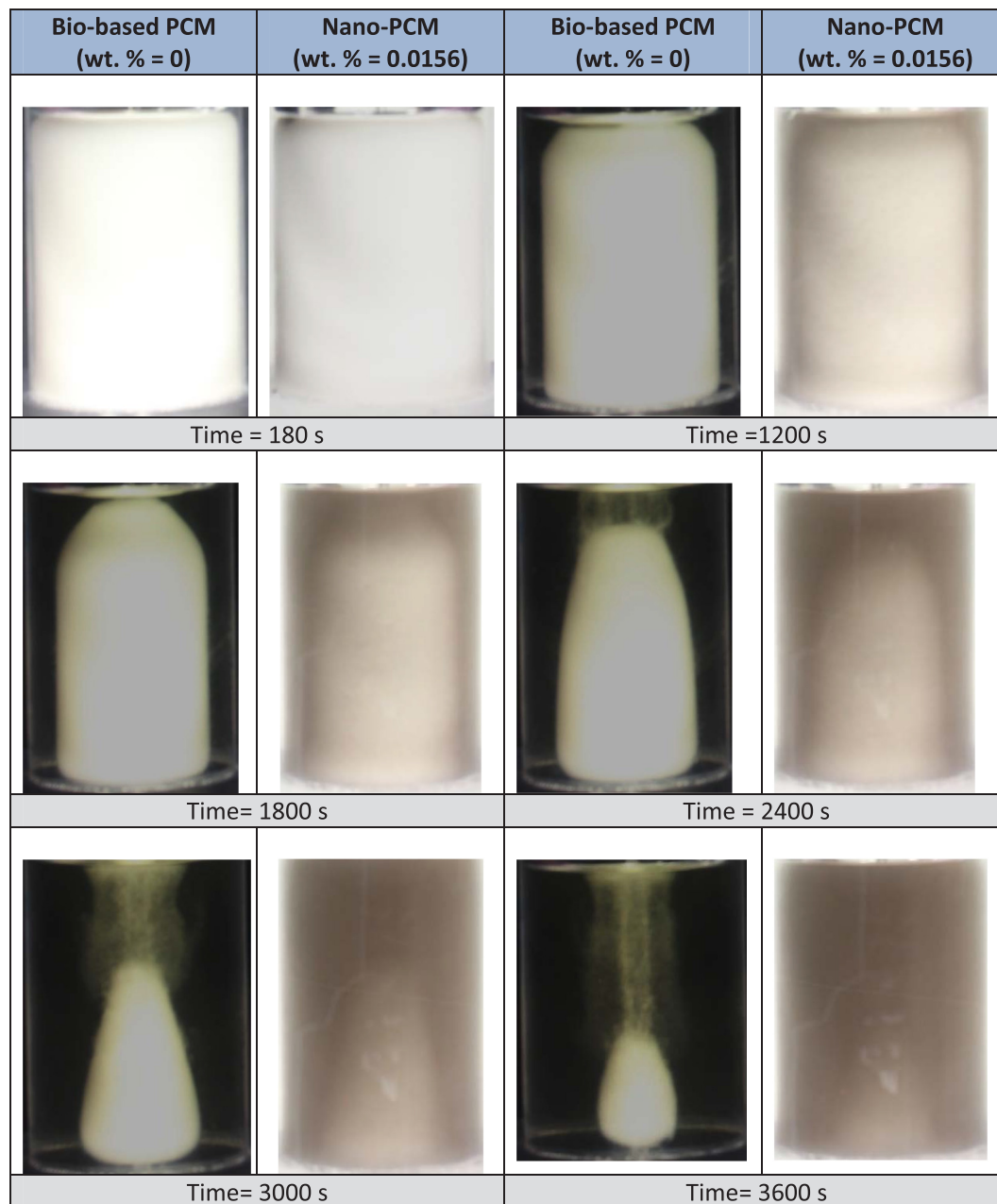


Fig. 5. Visualization comparison between bio-based PCM (wt.% = 0) and 0.0156 wt.% nano-PCM, H = 6 cm.

interface line near the top resulting in a dome shape solid PCM (see images at 1200 s). The combined domination of conduction and convection was continued as time advanced further. However, convection dominated more at the upper part with shrinking conduction dominating zone at the lower part as time advanced (see images at 1800 s). Strong convection current opens a large liquid PCM (and nano-PCM) region at the top of the C-TES system as can be seen from the images at 2400 s. Additionally, the thickness of the liquid layer close to the walls of C-TES system grew from the bottom to the top due the strong convection current. Concurrently, the shrinking solid PCM region at the center of the C-TES system took a shape similar to an inverted paraboloid, which reduced to a shape similar to a cone as time advanced further (see images at 3000 s and 3300 s). At the early stages of the melting process (up to 1200 s), adding nanoparticles did not show significant enhancement in the melting rate. After 1200 s, comparing with bio-based PCM, nano-PCMs melted faster. Additionally, it was observed that higher nanoparticle weight fractions led to faster melting

rate.

Calculating melt fraction requires accurate information on the amounts of liquid and solid forms of PCM at particular time during the melting process. Determining these amounts experimentally is a very challenging task due to the shape of the enclosure, color of the liquid and solid PCM, increasing turbidity in the liquid region due to the presence of nanoparticles, and non-uniformity in the interface region. Nevertheless, researchers have proposed different elegant methods for calculating melt fraction experimentally, these are namely volume based, surface based, and line based calculation methods ([20,22–24]). Each of these method has certain advantages and disadvantages. For example, Ho and Gao [20] used a volume based method to determine the amount of liquid nano-PCM. The authors quickly drained out the liquid nano-PCM at a particular time to record the liquid–solid interface. This method is extremely time consuming to have a complete melting picture, but accurate. In contrast, Fan et al. [22] used the volume expansion of the liquid PCM inside a narrow tube attached to their

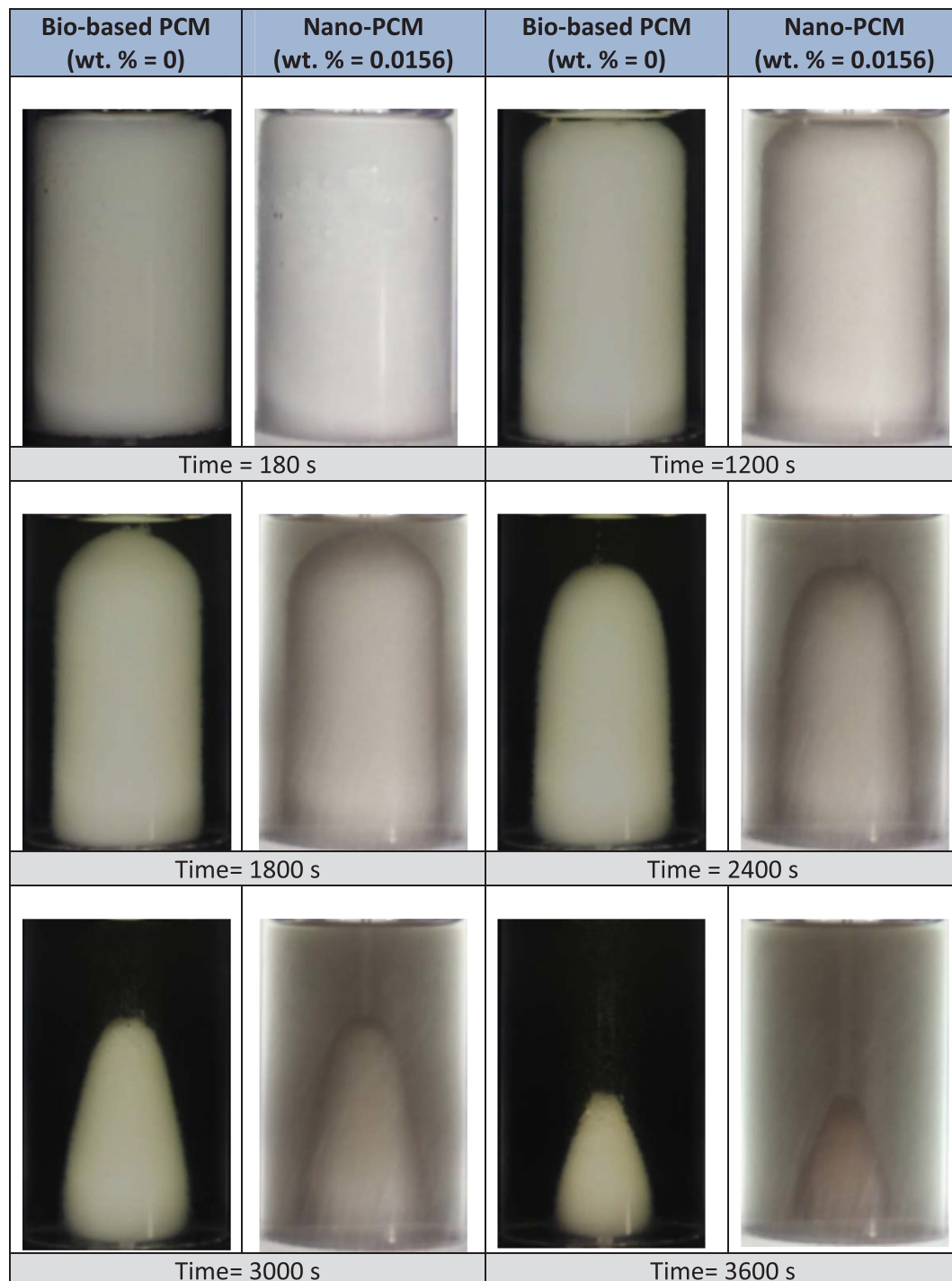


Fig. 6. Visualization comparison between bio-based PCM (wt.% = 0) and 0.0156 wt.% nano- PCM, H = 8 cm.

enclosure to calculate melt fraction during melting experiments. This indirect method has novelty when interfaces are hard to track due to the darkness of the nano-PCM. Shokouhmand and Kamkari [23] utilized the functionality of MATLAB image processing toolbox to calculate the melt fraction using the digital images from their experiments. Authors converted the color images to binary images (i.e., black pixels refer to 0 and white pixels refer to 1) after improving the contrast of the picture by filtering. This is an excellent method once one has quality 2-D images. However, pixels along the mushy zone may be a source of small error for this method. Al-Jethelah et al. [24] used a line method to track the solid–fluid interface using the magnified view of the experimentally obtained high quality 2-D images and then digitized the

tracked line along the interface to coordinate data points (i.e., x, y). A numerical integration is subsequently performed on the coordinated data points to calculate the solid and liquid areas of the digital images and, subsequently, the melt fraction. This method is extended further to calculate the volume of solid nano-PCM by revolving the digitally obtained surface as authors used an axi-symmetric geometry.

Fig. 3(a) presents a comparison of melt fraction between pure PCM and nano-PCMs for two different weight fractions (i.e., wt.% 0.0156 and wt.% 0.0218). To obtain the liquid melt fraction from the digital photos at different times, Grafula software was used. The melting images extracted by the digital camera were exported to the software interface. Next, the proper dimension of the C-TES system was defined



Fig. 7. Visualization comparison between bio-based PCM (wt.% = 0) and 0.0156 wt.% nano- PCM, H = 10 cm.

in the software environment. At the next step, a curvature was fitted along the solid–liquid interface of the PCM and nano-PCM from which co-ordinates data were extracted using Grafula’s digital data extraction feature. This resulted in the coordinates of each point on the curvature. Subsequently, the coordinates of each point were exported to Microsoft Excel spreadsheet for analysis and integration. From the interface coordinate data points a large number of area slices are considered and their areas and area-centers are determined. For all slices, the volumes generated due the 360° revolution are calculated and integrated to achieve the volume of the solid nano-PCM and subsequently the melt fraction. See Section 3.3 for discussion on the accuracy and uncertainty associated with this method.

Image processing method for calculating melt fraction was also used

by other researchers in literature, for example, Tan [25] calculated melt fraction inside a spherical container using the image processing method. The melt fraction proportionally increases with time for bio-based PCM and nano-PCMs. As it can be seen at the beginning of the melting process, pure PCM and nano-PCMs behaved almost the same. However, with an ongoing heating process, nano-PCMs melt faster than pure PCM.

In order to have a better comparison of melting pattern between bio-based PCM and nano-PCM, solid–liquid interface is presented further on the x-y plots. For a given height of the PCM/nano-PCM inside the C-TES system (H = 7.2 cm), transient evolution of the melting interface is presented in Fig. 3(b) for wt.% = 0.0218. The interface pattern associated with different regimes of melting (i.e., pure conduction,

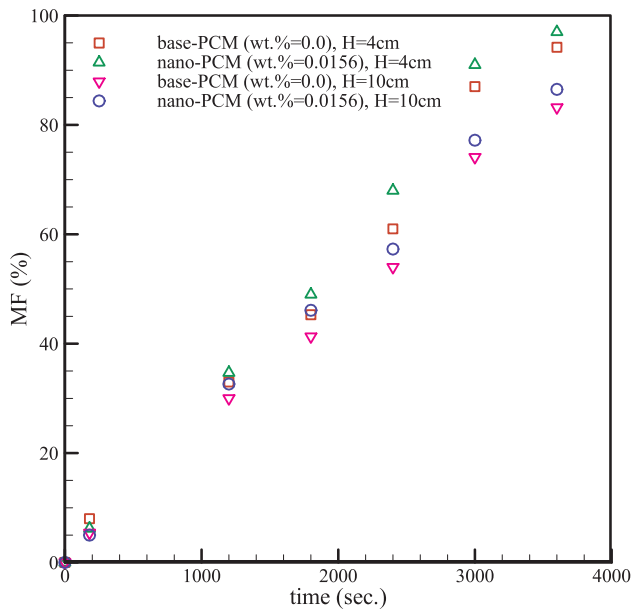


Fig. 8. Comparison of melt fraction between base-based PCM (wt.% = 0) and nano-PCM (wt.% = 0.0156) for different enclosure heights (H = 4 cm and H = 10 cm) and Th = 34 °C.

mixed convection and conduction, convection dominant and shrinking solid) is clearly visible in Fig. 3(b). Fig. 3(c) shows the effect of nanoparticle loading on the interface location at a selected time of melting (i.e., t = 2400 s.) and PCM/nano-PCM height (i.e., H = 7.2 cm) inside the C-TES system.

3.2. Visualization Experiments: wt.% = 0.0156 and H = 4 cm, 6 cm, 8 cm, and 10 cm

In another set of experiment, the effects of different heights (i.e. 4 cm, 6 cm, 8 cm, and 10 cm) of the filled nano-PCM representing the Rayleigh numbers of 1.38×10^6 , 4.7×10^6 , 1.11×10^7 , and 2.2×10^7 inside the C-TES system were examined for 34 °C wall temperature. To do so, the same procedure, as described in the previous section, was followed. As it can be seen from Figs. 4–7, there is a significant difference in the melting pattern occurring for different heights. For the lowest height of filled nano-PCM (i.e. H = 4 cm), the melting pattern tends to look like a dome shape. However, as the height increases, the solid part of the PCM tends to take the shape of an inverted paraboloid. Based on the shape of the solid PCM for different heights it can be concluded that the shape of the solid PCM depends on the distance between the domination of natural convection area, close to the upper part of the C-TES system, and the surface of the remaining solid PCM. Natural convection dominated at the upper part of the liquid PCM. At a height of 4 cm, the height of the liquid PCM was lower than those of higher heights (i.e. H = 6 cm to 10 cm) which made the strong convection currents closer to the solid PCM which affected the melting pattern. In addition, it was observed that increasing the height of the filled PCM, increased the melting time since more amount of PCM was used in the C-TES system. Besides, for the case of 4 cm, the difference between the remaining solid part of the bio-based PCM and nano-PCM was more significant. This can be a result of higher concentration of copper oxide nanoparticles at lower heights due to the sedimentation.

Fig. 8 shows the effect of the PCM height on the melt fraction (MF) of pure and nano-PCM (0.0156 wt.%). The comparison is between the PCM heights of 4 cm and 10 cm. As expected, increasing the PCM height increases its quantity, which requires more time to melt. Maximum increase in melt fraction is 15% for a wt.% = 0.0218 compared to the base case (wt.% = 0).

The experiment is conducted further considering two additional hot

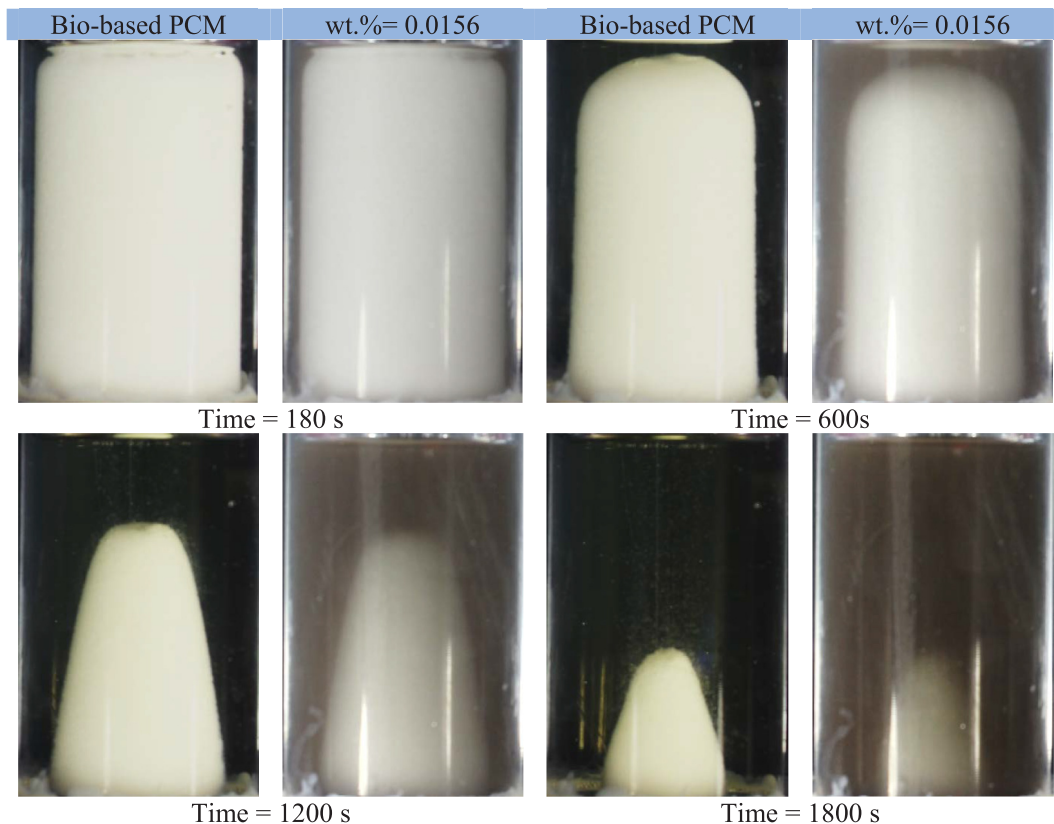


Fig. 9a. Visualization comparison of pure bio-based PCM (wt.% = 0) and nano-PCM (wt.% = 0.0156), Th = 44 °C and H = 7.2 cm.

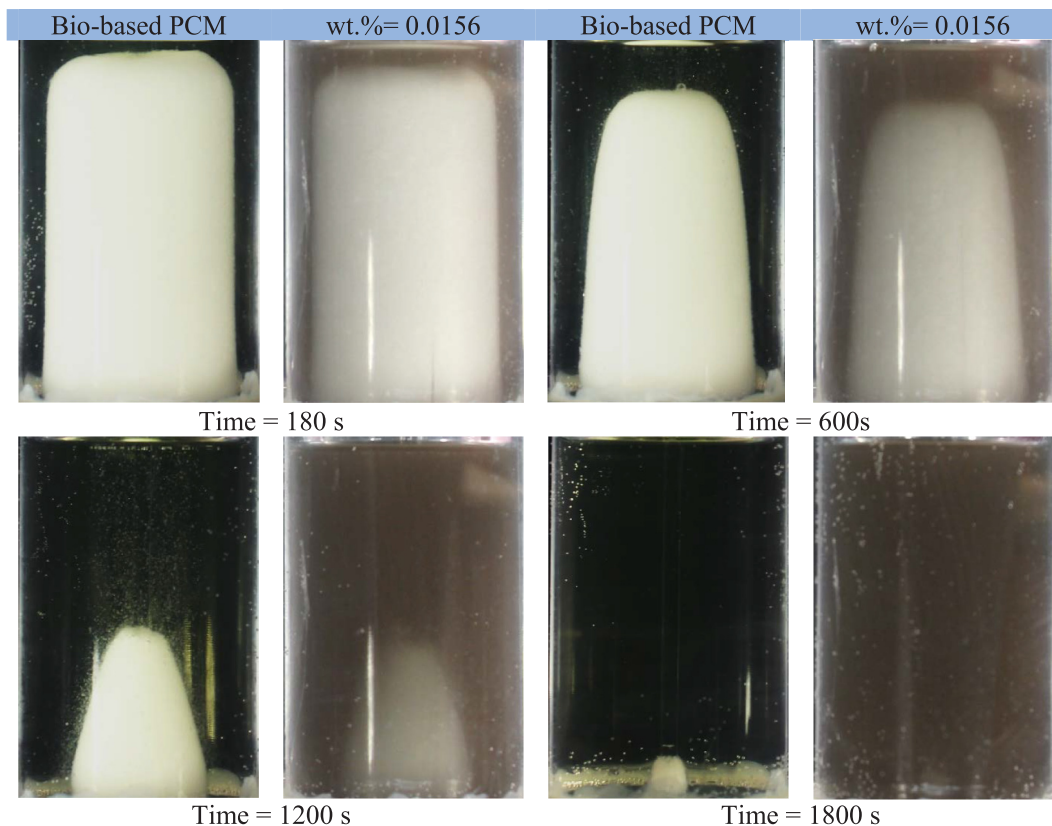


Fig. 9b. Visualization comparison of pure bio-based PCM (wt.% = 0) and nano-PCM (wt.% = 0.0156), $T_h = 54^\circ\text{C}$ and $H = 7.2\text{ cm}$.

wall temperatures (i.e., 44°C and 54°C). Melting images are captured at different times and some selected results are presented in Figs. 9a–9c. Rate of heat transfer increases at higher wall temperature which accelerates the melting process as can be observed from the images provided in Figs. 9a–9c.

3.3. Temperature measurement experiments

The transient temperature variations inside the bio-based PCM and nano-PCM are shown in Fig. 10(a) for a shorter C-TES system (i.e., $H = 6\text{ cm}$), while the variations for the taller C-TES system (i.e., $H = 10\text{ cm}$) are presented in Fig. 10(b). Effect of three different hot wall temperatures (i.e., 34°C , 44°C , and 54°C) is presented as well. To obtain the temperature profiles two C-TES systems were used simultaneously during the experiment as before; one system with bio-based PCM and the second one with nano-PCM of wt.% = 1.0. For each system, two T-type thermocouples were located in the center of each C-TES system at heights of 1.5 cm (T_{C1}) and 3.5 cm (T_{C2}) from the bottom of the C-TES system.

For all cases considered in Fig. 10, the initial temperature of the PCM and nano-PCM is 21°C . Once the wall temperature is raised to a specified value (i.e., 34°C), the solid phase of subcooled PCM and nano-PCM is heated up gradually through heat conduction process until the melting temperature is achieved. A lower slope in the temperature–time curve is an indication of the dominance of conduction heat transfer and the difference between the temperatures at two probe points remains fractionally small. As it can be observed, adding nanoparticles did not show significant effect on temperature variation at the conduction dominated phase. After the temperature of the PCM and nano-PCM reached to T_m , there is a significant change in the slope of curves, which is due to the onset of natural convection. Temperature increases rapidly at each probe point when the melting front as well as the natural convection thermal boundary layer moves over the probe points. Rapid

slope change occurs earlier for T_{C2} as this probe point is exposed to the melting front earlier. Effect of inclusion of nanoparticles is clearly visible at this convection dominated melting where the rapid rise in temperature at each probe points occurs at earlier time for nano-PCM than pure PCM. Adding nanoparticles to a PCM decreases the specific heat (c_p) and the latent heat of fusion (h) which reduces the sensible and latent heat capacity in the liquid PCM/nano-PCM. This results in higher temperature for the nano-PCM than that for bio-based PCM at the same time. However, according to a previous published work [25], this behavior also depends on the type of the PCM and nanoparticles. Towards the end of the melting process a second rapid slope change is observed in the temperature profiles. Each probe point temperature approaches to the wall temperature. An insignificant difference in the probe point temperatures is observed as the liquid PCM and nano-PCM nearly reach to the thermal equilibrium condition. Similar transient temperature–time profiles are observed for higher wall temperatures (i.e., 44°C and 54°C). The first and second drastic changes in the slope occur at earlier time when wall temperature is higher as melting front and thermal boundary layer pass earlier over the probe points at high wall temperature.

The impact of PCM height on the probe point temperature profiles are further clarified in Fig. 10(c), where transient temperature profiles are presented for $H = 6\text{ cm}$ and $H = 10\text{ cm}$ when wt.% = 0.0 and 1.0. As it can be observed from Fig. 10(c), the temperature of the PCM is higher as the height of the PCM is lower for both pure PCM and nano-PCM. As the height of the PCM is lower, the quantity of the PCM is less, which requires less heat for melting. Therefore, for a given wall temperature, first and second drastic changes in the slope in the temperature profiles occur at earlier time when $H = 6\text{ cm}$. The time it takes to raise the temperature above melting point increases by approximately 113% when the temperature of constant temperature bath is 54°C compared to 34°C and the height of the PCM is 6 cm for wt.% = 1. The time it takes to raise the temperature above melting point increases by

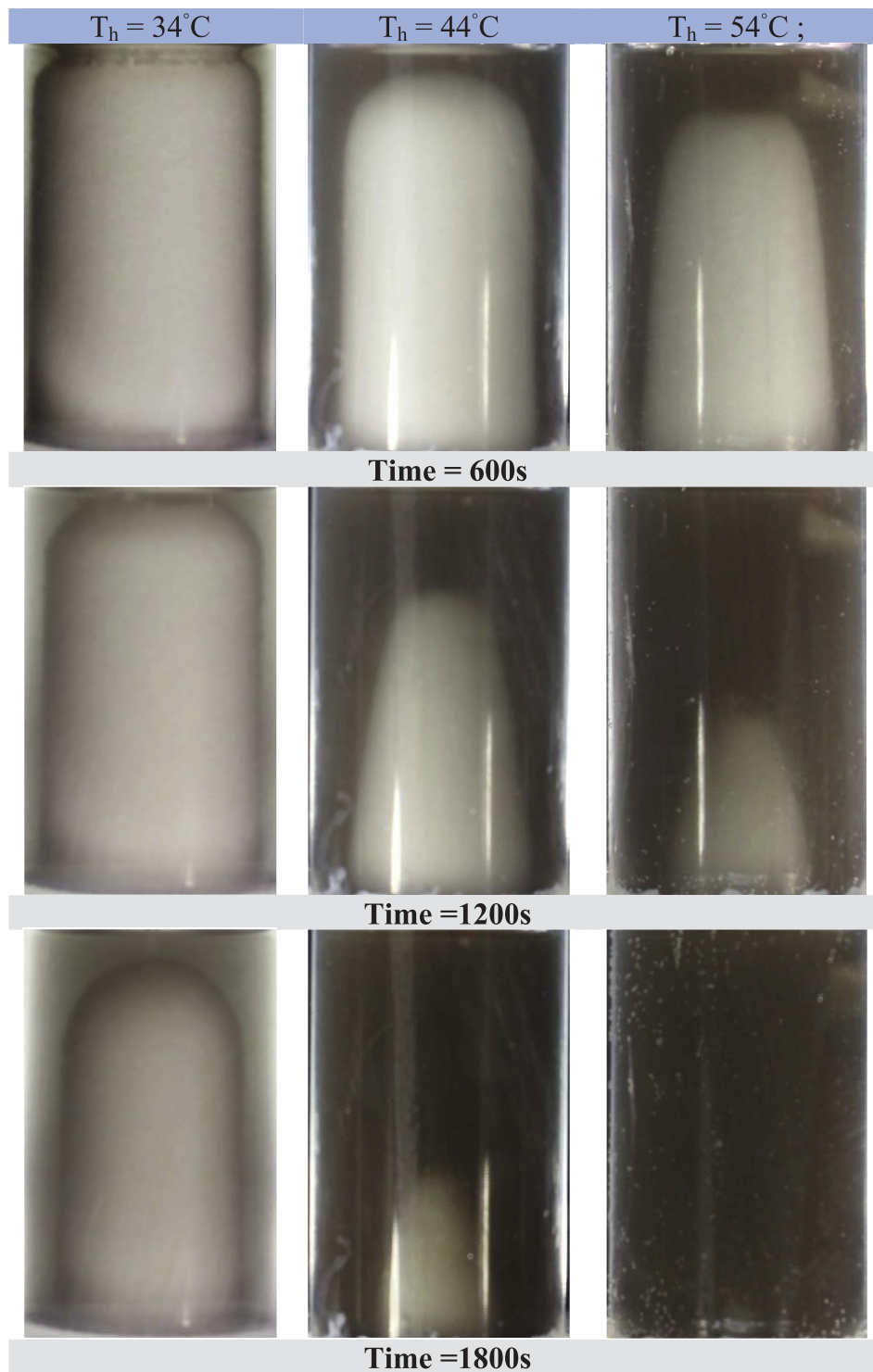


Fig. 9c. Visualization comparison of nano-PCM (wt.% = 0.0156) at $T_h = 34\text{ }^\circ\text{C}$, $44\text{ }^\circ\text{C}$, and $54\text{ }^\circ\text{C}$, $H = 7.2\text{ cm}$.

20% for a nano-PCM height of 10 cm compared to that of 6 cm for wt.% = 1. Higher wt.% of nanoparticles enhanced the rate of melting.

3.4. Uncertainty analysis of experimental results

In this section, an uncertainty analysis is performed to evaluate the accuracy of the results. This uncertainty is consisted of accuracy of the temperature measurement devices (i.e. thermocouples and DAQ system) and accuracy of the method used for calculating melting fraction from the digital photos.

The absolute measurement uncertainty (i.e., the accuracy) values for T-type thermocouples, DAQ system, and thermal regulator are $\pm 1\text{ }^\circ\text{C}$ ($= \delta T_{TC}$), $\pm 0.02\text{ }^\circ\text{C}$ ($= \delta T_{DQ}$), and $\pm 0.01\text{ }^\circ\text{C}$ ($= \delta T_{RG}$), respectively, where any quantity with the symbol δ represents the absolute measurement uncertainty. These values are provided by the manufacturers/suppliers of the equipment/sensors. The relative uncertainty of a measured quantity is estimated based on the propagation of uncertainty [22]. For example, the relative uncertainty associated with the nano-PCM temperature measurement inside the enclosure can be given by

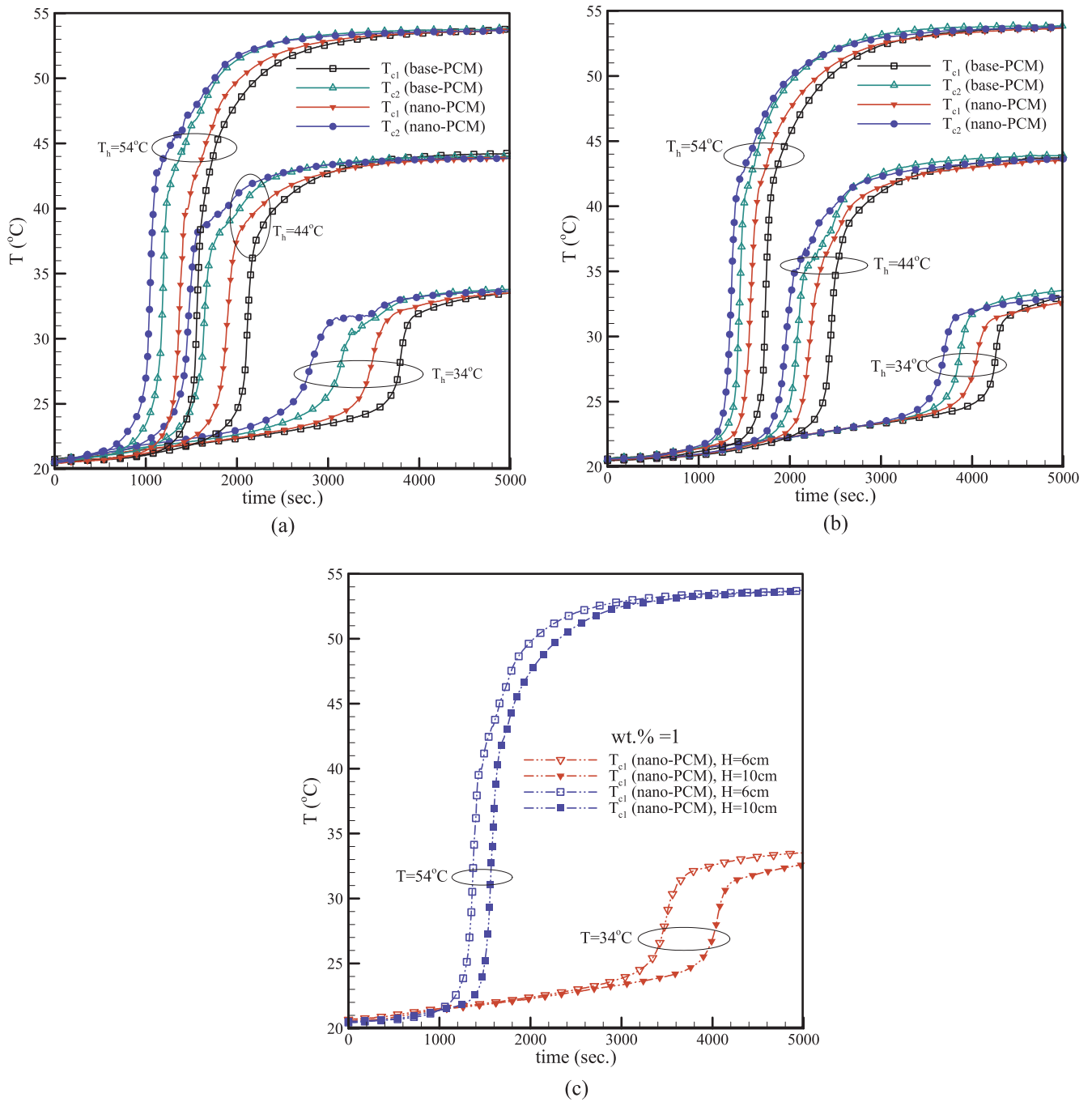


Fig. 10. Comparison of temperature profiles between bio-based PCM (wt.% = 0) and nano-PCM (wt.% = 1) at three different hot wall temperatures ($T_h = 34\text{ }^\circ\text{C}$, $44\text{ }^\circ\text{C}$, and $54\text{ }^\circ\text{C}$) and two heights ($H = 6\text{ cm}$ and 10 cm) of the enclosure (the thermocouple locations, T_{c1} and T_{c2} , are 1.5 cm and 3.5 cm from the bottom).

$$\frac{\delta T_c}{T_c} = \sqrt{\left(\frac{\delta T_{TC}}{T_{TC}}\right)^2 + \left(\frac{\delta T_{DQ}}{T_{DQ}}\right)^2} \quad (2)$$

For measured values of nano-PCM temperature of $21\text{ }^\circ\text{C}$ and $54\text{ }^\circ\text{C}$, the corresponding relative uncertainties are $\pm 4.76\%$ and $\pm 1.85\%$, respectively. Similarly, the relative uncertainty associated with the hot wall temperature measurement can be given by

$$\frac{\delta T_h}{T_h} = \sqrt{\left(\frac{\delta T_{RG}}{T_{RG}}\right)^2} \quad (3)$$

For measured values of hot wall temperatures of $34\text{ }^\circ\text{C}$ and $54\text{ }^\circ\text{C}$, the corresponding relative uncertainties are $\pm 0.03\%$ and $\pm 0.02\%$, respectively. Similarly, following equation can be used to determine the

relative uncertainty for total volume of the nano-PCM

$$\frac{\delta V}{V} = \sqrt{\left(\frac{\delta H}{H}\right)^2 + \left(2\frac{\delta D}{D}\right)^2} \quad (4)$$

where $\delta H = \delta D = \pm 0.1\text{ mm}$. For $H = 7.2\text{ cm}$ and $D = 4.44\text{ cm}$ the corresponding relative uncertainty for measuring total volume is $\pm 0.47\%$.

As discussed earlier a line based method [24] is used in this paper to calculate the melt fraction. High resolution images (i.e. 5187×3456 pixels) are taken by digital camera and processed them further for melt fraction calculation. A line based method is used to track the solid–fluid interface of the digital images to get the coordinate data points (i.e., x , y). From the interface coordinate data points a large number of area

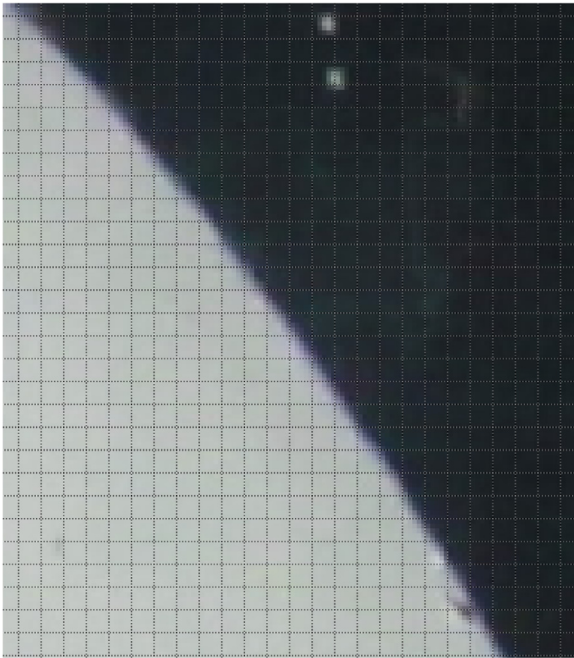


Fig. 11. Magnified view of a portion of the solid and liquid nano-PCM inside a pixel grid system.

slices, extended vertically upward, are calculated and their area centers are determined. For all slices, the volumes generated due the 360° revolution are calculated and added to achieve the volume of the solid nano-PCM. For this method, identifying the exact interface location is a very important step which is a source error for the co-ordinate data points. To elaborate the discussion further, a magnified view of a portion of the image taken during the experiment is shown in Fig. 11 where areas covered by both solid and liquid nano-PCM are captured inside a pixel grid system. A MATLAB image processing [23] can capture solid areas (brighter pixels) and liquid areas (darker pixels). However, the main uncertainty of image processing based calculation comes from the pixels representing the solid/liquid interface due to their partial darkness and partial brightness. This uncertainty will be more for the case of higher volume fraction of nanoparticles. A closer look at the interface reveals that the mushy zone does not extend more than 1 to 2 pixels and it remains within the 5-pixel grid block. Therefore, tracking interface with at least 1-pixel accuracy will give relatively accurate information on the interface location and subsequently the coordinate data points. For calculating the uncertainty associated with this method, the entire domain is initially divided into multiple sub-domains. In each domain, the average distance (in pixel) is calculated from the symmetry line to the interface. A line integration is performed to identify the area occupied by solid nano-PCM and then the average interface distance in pixel unit. Subsequently, following equation is used to calculate the relative uncertainty associated with the calculation of interface distance and co-ordinates:

$$\left(\frac{\delta x}{x}, \frac{\delta y}{y}\right) = \sqrt{\left(\frac{\delta N_{PX}}{N_{PX}}\right)^2}. \quad (5)$$

where δN_{PX} represents absolute measurement uncertainty at the interface in pixels. For example, when the average distances (in pixels), calculated from the symmetry line to the interface, is $N_{PX} = 92$ for the case shown in the Fig. 11, the corresponding value of $\delta x/x$ (or $\delta y/y$) is $\pm 1.08\%$ for $\delta N_{PX} = 1$, $\pm 2.17\%$ for $\delta N_{PX} = 2$, and $\pm 3.25\%$ for $\delta N_{PX} = 3$. Now, the relative uncertainty associated with the melt fraction calculation can be obtained from:

$$\frac{\delta MF}{MF} = \sqrt{\left(\frac{\delta x}{x}\right)^2 + \left(\frac{\delta y}{y}\right)^2 + \left(\frac{\delta \bar{x}}{\bar{x}}\right)^2 + \left(\frac{\delta V}{V}\right)^2}. \quad (6)$$

The corresponding value of $\delta MF/MF$ is $\pm 1.93\%$ for $\delta N_{PX} = 1$, $\pm 3.78\%$ for $\delta N_{PX} = 2$, and $\pm 5.64\%$ for $\delta N_{PX} = 3$. The relative uncertainty associated with the melt fraction calculation is higher towards the end of the melting process and the maximum value reaches to $\pm 6.7\%$.

4. Conclusion

The present study experimentally investigated the melting of a bio-based nano-PCM (i.e., copper oxide nanoparticles dispersed into coconut oil) in a vertical C-TES system with an aim to examine the effects of height of PCM, hot wall temperature, and loading of nanoparticles. The C-TES system was insulated from the bottom and isothermally heated from its sides. From the obtained results, the following conclusions can be drawn:

- The bio-based nano-PCM was prepared using magnetic stirring and sonication methods and its thermophysical properties were measured. Specific heat values of nano-PCM are decreased by 0.45% and 0.75%, compared to the base case for wt.% = 0.1 and 1, respectively. Thermal conductivity values of nano-PCM are increased by 4.8% and 7.5% compared to the base PCM for wt.% = 0.1 and 1, respectively. Latent heat of fusion values of nano-PCM are decreased by 1.94% and 8.25% compared to the base PCM for wt.% = 0.1 and 1, respectively.
- The mode of heat transfer significantly affects the shape of remaining solid PCM during melting. At the early stages, due to the dominance of conduction, the remaining solid PCM looked like a concentric cylinder. However, as the melting process evolved, the remaining PCM looked like the shape of a dome and inverted paraboloid. Moreover, the melting pattern was greatly depended on the height of filled PCM, which for lower heights tended to be dome-shaped and for higher heights to be inverted paraboloid-shape.
- The time requires to raise the temperature above melting point increases by 20% for a nano-PCM height of 10 cm compared to that of 6 cm for wt.% = 1.
- Higher wt.% of nanoparticles enhanced the rate of melting. Maximum increase in melt fraction is 15% for a wt.% = 0.0218 compared to the base case (wt.% = 0).
- The time requires to raise the temperature above melting point increases by approximately 113% when the temperature of constant temperature bath is 54 °C compared to 34 °C and the height of the nano-PCM is 6 cm for wt.% = 1.
- Image processing of photographs along with numerical integration is used to calculate melt fraction. To facilitate a better comparison of melting pattern between bio-based PCM and nano-PCM, solid–liquid interface is presented on the XY plots. An extensive analysis was reported as well to show how to calculate the uncertainty associated with image based melt fraction calculation. The relative uncertainty associated with the melt fraction calculation is higher towards the end of the melting process and the maximum value reaches to $\pm 6.7\%$.

Acknowledgement:

The corresponding author (S. Mahmud) acknowledges the financial support from Natural Sciences and Engineering Research Council of Canada through Discovery Grant and Ministry of Research and Innovation of Ontario through Early Researchers Award.

Appendix A. Supplementary material

Supplementary data associated with this article can be found, in the online version, at <https://doi.org/10.1016/j.applthermaleng.2018.05.091>.

References

- [1] A. Kumar, S.K. Shukla, A Review on thermal energy storage unit for solar thermal power plant application, *J. Energy Proc.* 74 (2015) 462–469.
- [2] B. Zalba, J. Marin, L.F. Cabeza, H. Mehling, A review on thermal energy storage with phase change materials: heat transfer analysis and applications, *Appl. Therm. Eng.* 23 (2003) 251–283.
- [3] G. Fang, H. Li, F. Yang, X. Liu, S. Wu, Preparation and characterization of nano-encapsulated *n*-tetradecane as phase change material for thermal energy storage, *J. Chem. Eng.* 153 (2009) 217–221.
- [4] N. Dhaidan, Nanostructures assisted melting of phase change materials in various cavities, *Appl. Therm. Eng.* 111 (2017) 193–212.
- [5] X. Zhang, X. Chen, Z. Han, W. Xu, Study on phase change interface for erythritol with nano-copper in spherical container during heat transport, *Int. J. Heat Mass Transf.* 92 (2016) 490–496.
- [6] R.K. Sharma, P. Ganesan, V.V. Tyagi, H.S.C. Metselaar, S.C. Sandaran, Thermal properties and heat storage analysis of palmitic acid-TiO₂ composite as nano-enhanced organic phase change material (NEOPCM), *Appl. Therm. Eng.* 99 (2016) 1254–1262.
- [7] S. Zhang, J. Wu, C. Tse, J. Niu, Effective dispersion of multi-wall carbon nano-tubes in hexadecane through physiochemical modification and decrease of super cooling, *Sol. Energy Mater. Sol. Cells* 96 (2012) 124–130.
- [8] N. Dhaidan, J. Khodadadi, Melting and convection of phase change materials in different shape containers: A review, *J. Renew. Sustain. Energy Rev.* 43 (2015) 449–477.
- [9] M. Jourabian, M. Farhadi, K. Sedighi, A. Rabienataj Darzi, Y. Vazifeshenas, Melting of NEPCM within a cylindrical tube: numerical study using the lattice boltzmann method, *Num. Heat Transfer, Part A: Appl.* 61 (2012) 929–948.
- [10] N. Dhaidan, J. Khodadadi, T. Al-Hattab, S. Al-Mashat, An experimental and numerical study of constrained melting of *n*-octadecane with CuO nanoparticle dispersions in a horizontal cylindrical capsule subjected to a constant heat flux, *Int. J. Heat Mass Transf.* 67 (2013) 523–534.
- [11] M. Bechiri, K. Mansouri, Analytical study of heat generation effects on melting and solidification of nano-enhanced PCM inside a horizontal cylindrical enclosure, *Appl. Therm. Eng.* 104 (2016) 779–790.
- [12] M. Jourabian, M. Farhadi, Melting of nanoparticles-enhanced phase change material (NEPCM) in a vertical semicircle enclosure: numerical study, *J. Mech. Sci. Technol.* 29 (9) (2015) 3819–3830.
- [13] Y. Zeng, L. Fan, Y. Xiao, Z. Yu, K. Cen, An experimental investigation of melting of nanoparticle-enhanced phase change materials (NePCMs) in a bottom-heated vertical cylindrical cavity, *Int. J. Heat Mass Transf.* 66 (2013) 111–117.
- [14] A. Sciacovelli, F. Colella, V. Verda, Melting of PCM in a thermal energy storage unit: numerical investigation and effect of nanoparticles enhancement, *Int. J. Energy Res.* 37 (13) (2013) 1610–1623.
- [15] H. Shamueli, G. Ziskind, R. Letan, Melting in a vertical cylindrical tubes: Numerical investigation and comparison with experiments, *Int. J. Heat Mass Transf.* 53 (2010) 4082–4091.
- [16] E.M. Sparrow, J.A. Broadbent, Inward melting in a vertical tube which allows free expansion of the phase-change medium, *J. Heat Transfer* 104 (1982) 309–315.
- [17] C. Wenzhen, C. Shangmo, L. Zhen, G. Wangmin, Study of contact melting inside isothermally heated vertical cylindrical capsules, *J. Therm. Sci.* 2 (1993) 190–195.
- [18] B. Jones, D. Sun, S. Kishan, S. Garimella, Experimental and numerical study of melting in a cylinder, *Int. J. Heat Mass Transf.* 49 (2006) 2724–2738.
- [19] S. Ebadi, S.H. Tasnim, A.A. Aliabadi, S. Mahmud, Melting of nano-PCM inside a cylindrical thermal energy storage system: Numerical study with experimental verification, *Energy Convers. Manag.* 166 (2018) 241–259.
- [20] C.J. Ho, J.Y. Gao, An experimental study on melting heat transfer of paraffin dispersed with Al₂O₃ nanoparticles in a vertical enclosure, *Int. J. Heat Mass Transf.* 62 (2013) 2–8.
- [21] M.M. Farid, A.M. Khudhair, S.A.K. Razack, S. Al-Hallaj, A review on phase change energy storage: materials and applications, *Energy Convers. Manag.* 45 (2004) 1597–1615.
- [22] Li-Wu Fan, Zi-Qin Zhu, Yi Zeng, Q. Ding, Min-Jie Liu, Unconstrained melting heat transfer in a spherical container revisited in the presence of nano-enhanced phase change materials (NePCM), *Int. J. Heat Mass Transf.* 95 (2016) 1057–1069.
- [23] H. Shokouhmand, B. Kamkari, Experimental investigation on melting heat transfer characteristics of lauric acid in a rectangular thermal storage unit, *Exp. Therm Fluid Sci.* 50 (2013) 2001–2012.
- [24] M. Al-Jethelah, S.H. Tasnim, S. Mahmud, A. Dutta, Nano-PCM filled energy storage system for solar-thermal applications, *Renew. Energy* 126 (2018) 137–155.
- [25] F.L. Tan, Constrained and unconstrained melting inside a sphere, *Int. Commun. Heat Mass Transfer* 35 (2008) 466–475.